JOURNAL OF GUIDANCE, CONTROL, AND DYNAMICS
Vol. 31, No. 5, September–October 2008

Reentry Flight Clearance Using Interval Analysis

S. Juliana,* Q. P. Chu,† and J. A. Mulder‡
Delft University of Technology, 2629 HS Delft, The Netherlands

DOI: 10.2514/1.34091

Reentry flight is one of the most challenging parts in spaceflight missions. Before the actual flight, the vehicle has to be certified for safety of flight within its intended flight domain. This certification process, called reentry flight clearance, is based on accurate mathematical models of the vehicle and its environment. Current practice is to use model evaluations including a representative set of uncertainty parameter combinations in a Monte Carlo approach. The objective of the present paper is to evaluate the application of a promising new mathematical technique called interval analysis for reentry flight clearance. Whereas a Monte Carlo approach clears the vehicle only for a finite number of sets of uncertainty parameters, the new approach clears the vehicle within prespecified uncertainty parameter intervals. The new approach is applied to the reentry trajectory of the Delft Aerospace Reentry Test Demonstrator, a hypothetical ballistic reentry vehicle equipped with an attitude-stabilizing flight control system. As the clearance requirement, the stability of the system is chosen, which is evaluated using two different mathematical criteria: worst-case linear eigenvalue analysis and nonlinear Lyapunov analysis. The new approach, based on interval analysis, is applied in an evaluation of both criteria. Subsequently, Monte Carlo analysis was performed to verify the validity of these results.

I. Introduction

REENTRY flight is inseparable from the present and future spaceflight missions. During the reentry flight, a vehicle has to follow a predefined trajectory toward a designated landing area. Trajectory tracking, flight stability, and landing precision are important aspects in the reentry flight. The predefined trajectory has to be tracked with a sufficient margin of error. The stability margin has to be fulfilled against the variation and uncertainty in flight parameters such as aerothermodynamic parameters, mass, and inertia. The accuracy of landing is important as well to ensure that the vehicle and its contents reach the target ground intact. All of these aspects need to be analyzed and evaluated in a systematic way to ensure the stability and performance of the reentry vehicle.

To certify a reentry vehicle as safe to fly, the reentry flight model has to be evaluated before actual flight. This is known as the reentry flight model clearance, or reentry flight clearance for short. One example of the flight model clearance is the evaluation of the stability and performance of the reentry vehicle model in its flight envelope. As illustrated in Fig. 1, the reentry flight envelope is defined along the nominal flight trajectory. The flight safety is checked by evaluating the regions in the flight envelope using predefined stability or performance criteria. The region in which the criteria are fulfilled is then "cleared," which means that, under the defined flight condition, the vehicle can fly safely in this region. The right-hand side of Fig. 1 shows a blown-up view of the envelope with flyable and nonflyable regions as a result of the clearance. The flyable areas are shown by the shaded rectangles in the flight envelope.

The challenge for the reentry flight clearance lies in the fact that the mathematical models of reentry vehicles and the environments are generally nonlinear. Moreover, the models may contain uncertainty due to the unknowns and variations in the dynamics or parameters. Therefore, to produce a reliable clearance result, mathematical analysis methods that account for the nonlinearity and uncertainty in the models are needed. To answer this question, this paper contributes a systematic approach to perform reentry flight clearance using interval analysis. This method can meet the aforementioned challenge, for it can be applied to linear as well as nonlinear systems, and can account for the uncertainty in the system model.

To give the reader an overview of the method, the algorithm is described in Sec. V. The strong point of the method is illustrated using an example of clearance for a nonlinear system. In the sequence, we perform clearance on a reentry vehicle model with a flight control system, with stability robustness in the presence of uncertainty as the clearance criteria (see Sec. VI). The mathematical model of the system is nonlinear with uncertain parameters. To show that the method can be applied to linear as well as nonlinear systems, both linearized and nonlinear models of the system are evaluated. The clearance is performed inside the vehicle's reentry flight envelope. For the linearized system, the eigenvalue criteria is applied, whereas for the nonlinear system, the Lyapunov function is evaluated. The results are validated using Monte Carlo analysis. As literature survey, Secs. II and III provide the reader with an overview of the current clearance practice and of the available methods, which leads to the choice of the clearance method in this paper.

II. Flight Clearance Practice

The usual flight clearance practice is performed by combining computational and experimental approaches. These include mathematical analyses, computer simulations, and flight tests.

In flight clearance using mathematical analyses, the characteristics of a vehicle are evaluated by analyzing its mathematical model according to some predefined clearance criteria (e.g., stability and performance criteria). This clearance approach is also called mathematical clearance. The use of mathematical analyses for a clearance process has been shown applicable to atmospheric flight (see, e.g., [1]). As shown in this paper, the approach is also applicable to reentry flight vehicles.

Another flight clearance approach is using computer simulations based on the Monte Carlo analysis. In this approach, a set of system models are run in a simulation environment. To obtain adequate result accuracy, the simulations have to include various combinations of parameters considered to be critical according to the clearance criteria; therefore, a large number of simulations are required.

Presented as Paper 6780 at the AIAA Guidance, Navigation, and Control Conference, Hilton Head, South Carolina, 20–23 August 2007; received 17 August 2007; accepted for publication 12 November 2007.

*Research Associate, Control and Simulation Division, Faculty of Aerospace Engineering, Kluyverweg 1. Member AIAA.

†Associate Professor, Control and Simulation Division, Faculty of Aerospace Engineering, Kluyverweg 1. Member AIAA.

‡Professor, Chairman of the Control and Simulation Division, Faculty of Aerospace Engineering, Kluyverweg 1. Member AIAA.

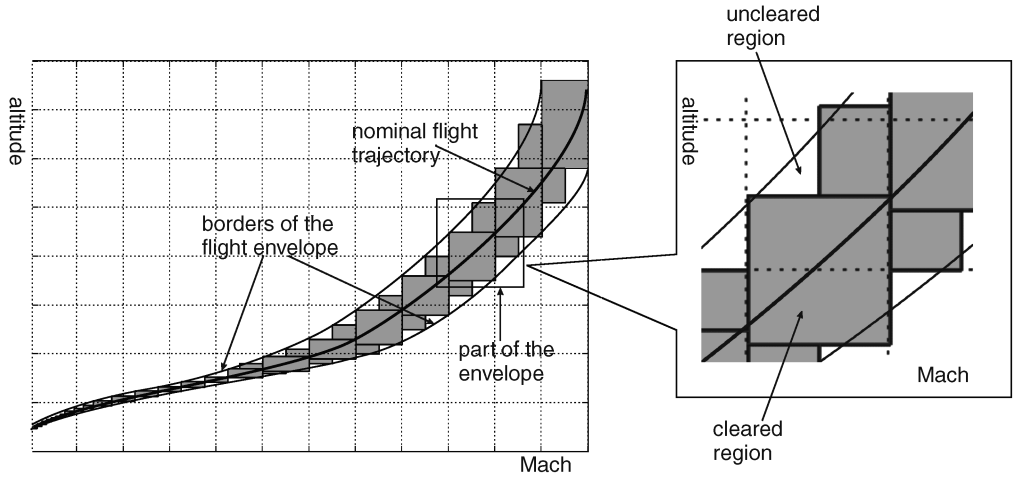

Fig. 1 Illustration of reentry flight envelope clearance.

Some examples of clearance using Monte Carlo simulations are the assessments of trajectory dispersion for several reentry vehicles given by [2–5]. The purpose of the simulations was to estimate the downrange and cross range of the landing area. The statistical results of the landing dispersions were obtained after thousands of numerical simulations involving variations in parameters. Another example of Monte Carlo simulations is the flight envelope clearance for the Mu Space Engineering Spacecraft (MUSES-C) asteroid explorer given by [6]. The objective of the clearance was to assess the attitude stability of the reentry capsule in the early phase of reentry, that is, in a hypersonic rarefied flight region. In the simulations, numbers of variations of altitude, velocity, pressure, and temperature were taken into account. Pitching motion of the MUSES-C capsule can be stabilized in the early phase of reentry by initiating a spinning motion around the capsule axis at an appropriate frequency [6].

The third approach, flight test, can be considered as the most accurate approach to perform flight clearance, because the vehicle is evaluated in the actual flight conditions. A large number of trials are required to cover the variations in flight parameters. This approach is not common for reentry flight clearance, because the cost involved in the tests is very high. Until recently, flight tests for the reentry flight clearance were performed only for a partial flight region, not the entire reentry trajectory. One example of such flight tests is presented in [7]. The objective of these flight tests was to evaluate the dynamic stability of reentry vehicles in the atmospheric region. For this evaluation, 83 flight tests were performed on 6 scaled models, which were designed based on the Huygens, Mars Microprobe, Stardust, and Genesis reentry vehicles. The tests were conducted from Mach numbers 0.7 to 3.5; hence, they did not cover the hypersonic flight regime.

III. Mathematical Clearance Methods

Recent development in the clearance of flight control laws is described in [8]. The work was applied to a military aircraft with a flight control system. The research was aimed to provide fast, efficient, and numerically reliable analysis tools for the clearance process.

In general, the characteristics of computational clearance methods can be distinguished according to the types of numerical analysis to be performed, which are discrete and continuous, and the types of system to be handled (or criteria to be used), which are linear and nonlinear. Discrete analysis is also known as the grid-point method, in which the models to be analyzed are divided into a set of grid points in the operational domain. As a result, a set of models are obtained and each can be analyzed separately. To increase the accuracy of the analysis, finer grid points are necessary. For continuous analysis, on the other hand, the models need not be divided into separate grid points. Therefore, continuous analysis is in principle more accurate than discrete analysis.

The classical flight clearance process using the discrete or grid-point approach is usually performed in several steps [1]. First, system models, possibly nonlinear, with or without control systems, are generated. The engineers familiarize themselves with these models and perform a trend study on the effects of uncertain parameters to the models, for example, to the stability and performance characteristics. In the next step, the models are linearized. If stability is the clearance criteria, then stability analysis is performed by calculating the stability margin on a set of grid points in the flight region. Finally, nonlinear simulations may be performed to verify the clearance results. The accuracy of discrete analysis can be improved by making finer grids; as a consequence, however, the computation time will increase. Despite these disadvantages, discrete analysis might be preferable in certain applications due to its simplicity. In the industry, clearance practice still relies heavily on the discrete type of analysis, in which a large number of flight conditions are taken and Monte Carlo analysis or powerful linear analysis tools are applied.

According to [9], several more advanced approaches have been developed for the mathematical clearance process, which are as follows: 1) μ analysis [10], 2) bifurcation and continuation method [11], 3) interval analysis [12], 4) ν-gap analysis [13], and 5) optimization-based analysis [14].

The references on all above-mentioned items describe the characteristics of each method in detail, together with its advantages and drawbacks. The characteristics of the computational clearance methods can be summarized in Table 1.

Table 1 Categorization of the mathematical clearance methods

	Linear	Nonlinear	Discrete/Grid	Continuous
Grid-point analysis	×	——	×	——
Monte Carlo analysis	×	×	×	——
μ analysis	×	——	×	——
ν-gap analysis	×	——	×	——
Bifurcation and continuation	——	×	——	×
Interval analysis	×	×	×	×
Optimization-based analysis	×	×	×	×

Clearance process using a linear method is simpler than using a nonlinear method. Therefore, sometimes a nonlinear system is modeled as a linear system by trimming and linearization to make a linear clearance method applicable. In this way, considerable time and effort can be saved. The result accuracy, however, might be lower than when using a nonlinear clearance method.

The reentry vehicle dynamics are generally nonlinear and change rapidly with time. Thus, it is desirable that the clearance methods to be used are capable of dealing with nonlinear models. It is also preferable that the methods are suitable for continuous analysis, because higher result accuracy can be expected when continuous analysis is used instead of discrete analysis. According to Table 1, there are three methods that can cope with nonlinear and continuous system analysis: bifurcation and continuation method, interval analysis, and optimization-based analysis. The reliability of bifurcation and continuation method is considered low because it cannot guarantee the finding of worst cases [9]. Interval analysis offers possibilities to solve for any clearance criteria, linear or nonlinear, which can be expressed in the form of algebraic function. The optimization-based analysis translates the clearance criteria into an optimization problem. If no global optimization algorithm is available, worst cases can be missed [9]. Comparing the main properties of the three methods, it appears that interval analysis is more suitable for reentry flight clearance application than the other two. Therefore, interval analysis was chosen to be used in this research.

IV. Clearance for Nonlinear Systems

The problem of clearance for nonlinear systems can be illustrated in the following. Consider a nonlinear system model

$$\dot{x} = -\theta x + x^2, \qquad \theta > 0 \tag{1}$$

where x is the state variable and θ is a constant uncertain parameter. This system has two equilibria, namely, $x_{10} = 0$ and $x_{20} = \theta$. The first equilibrium is stable, whereas the second is unstable. We are interested in knowing the stability of the system around the equilibria, that is, to clear the space around these points that meets the stability criteria. The stability of this system depends on the initial condition of the state variable as well as on the value of θ, as shown by the time responses of the system in Fig. 2. Clearance of the system can be performed to obtain the stability domain of this system as follows.

Assume that the parameter θ contains an unknown but bounded uncertainty. The uncertain parameter can be expressed as

$$\theta = \theta_0(1 + \delta_\theta) \tag{2}$$

with θ_0 the nominal value of θ and δ_θ the uncertainty, which may vary within the interval

$$\delta_\theta \in [\underline{\delta}_\theta, \bar{\delta}_\theta] \tag{3}$$

Using the expression for the uncertain parameter in Eq. (2), the expression for the nonlinear system in Eq. (1) can be modified as

$$\dot{x} = -\theta_0(1 + \delta_\theta)x + x^2 \tag{4}$$

To analyze the stability of the system in Eq. (1), one can use the nonlinear analysis method. Alternatively, we also can linearize the system on the operating points and use the linear method to analyze the stability of the system. The second method has its advantage as well as limitation. To illustrate the limitation of the linear stability analysis for this nonlinear system, let us consider a linearized model of the system. The system in Eq. (1) is linearized at the equilibrium $x_{10} = 0$. The linearized system can be written as

$$\dot{x} = -\theta x, \qquad \theta > 0 \tag{5}$$

Figure 3 shows the time responses of the linearized system for various initial conditions. Independent of the initial states, the responses of $x(t)$ always converge to the equilibrium point $x_{10} = 0$.

By inspecting Figs. 2 and 3, it can be concluded that the linear stability analysis is only valid for $x \leq \theta$. However, the linear simulations give no indication of this limit. We can conclude from this example that one has to be aware of the limitation of linear stability analysis when applying it to nonlinear systems.

Let us consider the nonlinear system described by Eq. (4). As the value of the parameter θ is uncertain, the equilibrium point $x_{20} = \theta$ cannot be determined accurately. To know the stability of the nonlinear system in the presence of uncertainty in θ, a systematic analysis has to be performed. This involves two main steps: first, the definition of the stability criteria, and second, the evaluation of the criteria using a suitable method.

For the first step, the stability of the system in the presence of the uncertainty, can be determined by using a Lyapunov function analysis. Take a Lyapunov function candidate for the system in Eq. (4) as

$$V = \tfrac{1}{2}x^2 \tag{6}$$

The function V is positive definite for all x. Its first-order derivative can be written as

$$\dot{V} = x\dot{x} = -\theta_0(1 + \delta_\theta)x^2 + x^3 \tag{7}$$

There is generally no effective method to construct the Lyapunov function. Therefore, a trial-and-error approach is usually employed

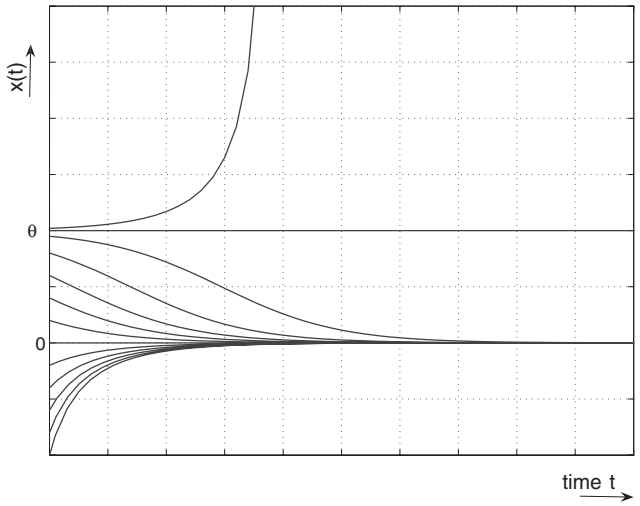

Fig. 2 Time responses of the system in Eq. (1) for various initial conditions.

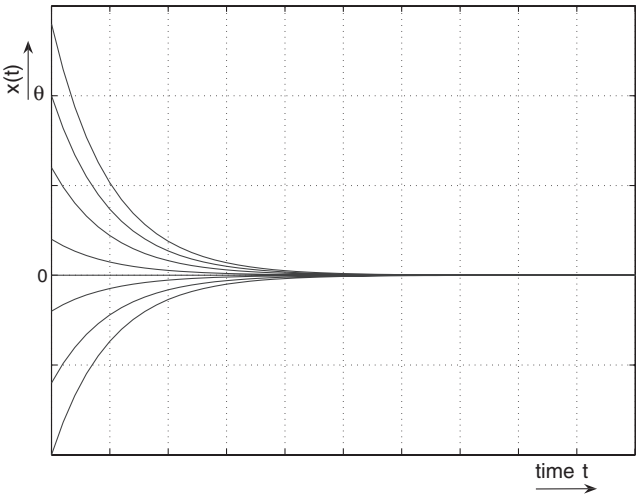

Fig. 3 Time responses of the linearized system in Eq. (5) for various initial conditions.

to find it. Fortunately, for mechanical systems, the energy-conservation principle can be used to form a suitable choice of the Lyapunov function.

As the clearance criterion, the system is robustly stable in the presence of the uncertainty δ_θ if the derivative of the Lyapunov function, that is, $\dot{V}$ in Eq. (7), is negative semidefinite for all combinations of x and θ. Defining a parameter set

$$P = \{x, \theta\} \tag{8}$$

we are interested in checking whether the function $\dot{V}$ is negative semidefinite in the whole domain of P. In other words, the stability domain can be defined as

$$\mathbb{S}_P \equiv \{P \in \mathbb{R}^2 | \dot{V}(p) \leq 0\} = \dot{V}^{-1}(]-\infty, 0]) \tag{9}$$

The characterization of $\mathbb{S}_P$ can be cast into the framework of set inversion and performed by the interval analysis algorithm presented in the next section.

Note that the existence of the Lyapunov function gives a sufficient condition of stability. This gives conservatism to the result, because only a positive result is guaranteed. For clearance purposes, this means that when the stable domain is found, it is guaranteed to be correct. However, the noncleared regions are not necessarily unstable. To further examine the noncleared region, other Lyapunov function candidates have to be evaluated.

V. Clearance Algorithm Using Interval Analysis

Interval analysis was invented to do numerical operations for intervals of numbers instead of for numbers themselves to avoid errors caused by measurement, approximation, or rounding [15,16]. The applications of this method have been developed in many fields (see, e.g., [17–20] and many others). For the basics of interval analysis, the reader is referred to the available literature, for example, [15], which provides extensive discussions on the topic.

The algorithm used for this paper is called set inversion via interval analysis (SIVIA) [17]. Two important notions in the algorithm are presented here, namely the inclusion function and subpaving. The inclusion function is defined as follows [21]. Consider a function $\mathbf{f}$ from $\mathbb{R}^n$ to $\mathbb{R}^m$. The interval function $[\mathbf{f}]$ from $\mathbb{IR}^n$ to $\mathbb{IR}^m$ is an *inclusion function* for $\mathbf{f}$ if

$$\forall\ [\mathbf{x}] \in \mathbb{IR}^n, \qquad \mathbf{f}([\mathbf{x}]) \subset [\mathbf{f}]([\mathbf{x}]) \tag{10}$$

The purpose of interval analysis is, among other things, to provide, for a large class of $\mathbf{f}$, inclusion functions that can be evaluated quickly and are not too large. An inclusion function $[\mathbf{f}]$ of $\mathbf{f}$ allows one to compute a box $[\mathbf{f}]$ $([\mathbf{x}])$ such that $\mathbf{f}([\mathbf{x}])$ is contained in $[\mathbf{f}]$ $([\mathbf{x}])$.

Figure 4 illustrates the notion of the inclusion functions. It is the plot of a mapping from $\mathbb{R}^2$ to $\mathbb{R}^2$ by a function $\mathbf{f}$. The image set $\mathbf{f}([\mathbf{x}])$ may be nonconvex or even disconnected if $\mathbf{f}$ is discontinuous. Regardless of this fact, an inclusion function $[\mathbf{f}]$ of $\mathbf{f}$ allows one to compute a box $[\mathbf{f}]$ $([\mathbf{x}])$ such that $\mathbf{f}([\mathbf{x}])$ is contained in $[\mathbf{f}]$ $([\mathbf{x}])$.

The inclusions may be pessimistic, as shown by the outer box $[\mathbf{f}]$ $([\mathbf{x}])$ in Fig. 4. The smallest box that contains $\mathbf{f}([\mathbf{x}])$ is called the minimal inclusion function for $\mathbf{f}$, denoted by $[\mathbf{f}]^*$ $([\mathbf{x}])$ in Fig. 4. The minimal inclusion function is unique.

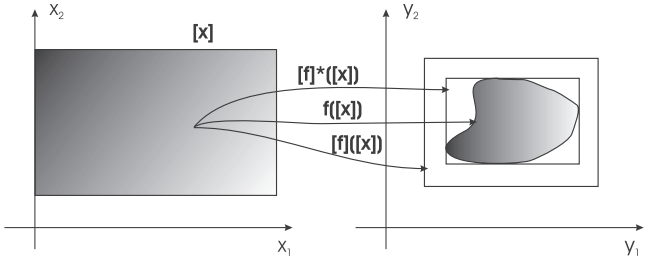

Fig. 4 Illustration of the inclusion functions.

The notation of subpaving is defined as follows [22]. Take a set of interest $\mathbf{X}$ within $\mathbb{R}^n$. This set is included between its inner and outer approximations, that is,

$$\underline{\mathbf{X}} \subset \mathbf{X} \subset \bar{\mathbf{X}} \tag{11}$$

The knowledge of the inner and outer approximations provides some valuable information about $\mathbf{X}$. This set can be covered with sets of nonoverlapping boxes of $\mathbb{R}^n$, which are called *subpavings*.

A subpaving of $[\mathbf{x}]$ is regular if each of its boxes can be obtained from $[\mathbf{x}]$ by a finite succession of bisections and selections. Figure 5 illustrates a regular paving of the box $[\mathbf{x}] = [a, c] \times [a, c]$. The gray boxes form a regular subpaving Q of $[\mathbf{x}]$, where

$$Q = [a, b] \times [a, b] \cup [b, d] \times [b, c] \cup [d, e] \times [b, d] \cup [d, e] \times [d, e] \tag{12}$$

Set inversion is defined as follows. Let $\mathbf{f}$ be a possibly nonlinear function from $\mathbb{R}^n$ to $\mathbb{R}^m$, and let $\mathbf{Y}$ be a subset of $\mathbb{R}^m$. The set inversion is the computation of the reciprocal image

$$\mathbf{X} = \{\mathbf{x} \in \mathbb{R}^n | \mathbf{f}(\mathbf{x}) \in \mathbf{Y}\} = \mathbf{f}^{-1}(\mathbf{Y}) \tag{13}$$

of a regular subpaving $\mathbf{Y} \subset \mathbb{R}^m$ by a function $\mathbf{f}$:$\mathbb{R}^n \to \mathbb{R}^m$. The algorithm serves as a method to compute two subpavings $\underline{\mathbf{X}}$ and $\bar{\mathbf{X}}$ of $\mathbb{R}^n$, such that Eq. (11) is satisfied.

The algorithm has been developed in [17] to obtain the subpavings in Eq. (11) for $\mathbf{X}$, for any function $\mathbf{f}$ with a convergent inclusion function $[\mathbf{f}]$. Four cases can be encountered in the algorithm:

1) $[\mathbf{f}]$ $([\mathbf{x}])$ has a nonempty intersection with $\mathbf{Y}$, but is not entirely in $\mathbf{Y}$. The set $[\mathbf{x}]$ then may contain part of the solution set; it is said to be *undetermined*. If the magnitude of $[\mathbf{x}]$ is larger than a predefined small number ϵ, the algorithm bisects the interval. The test is further performed recursively on the newly generated intervals.

2) $[\mathbf{f}]$ $([\mathbf{x}])$ has an empty intersection with $\mathbf{Y}$,

$$[\mathbf{f}]([\mathbf{x}]) \cap \mathbf{Y} = \emptyset \tag{14}$$

This means that $[\mathbf{x}]$ does not belong to the solution set.

3) $[\mathbf{f}]$ $([\mathbf{x}])$ is entirely in $\mathbf{Y}$,

$$[\mathbf{f}]([\mathbf{x}]) \subset \mathbf{Y} \tag{15}$$

Therefore, $[\mathbf{x}]$ belongs to the solution and is stored in $\underline{\mathbf{X}}$ and $\bar{\mathbf{X}}$, that is,

$$\{\underline{\mathbf{X}} := \underline{\mathbf{X}} \cup [\mathbf{x}]; \bar{\mathbf{X}} := \bar{\mathbf{X}} \cup [\mathbf{x}]\} \tag{16}$$

4) The interval $[\mathbf{x}]$ is undetermined, whereas its width is smaller than a predefined small number ϵ,

$$w([\mathbf{x}]) < \epsilon \tag{17}$$

As the interval is small enough, it can be stored in the outer approximation $\bar{\mathbf{X}}$ of $\mathbf{X}$, that is,

$$\{\bar{\mathbf{X}} := \bar{\mathbf{X}} \cup [\mathbf{x}]\} \tag{18}$$

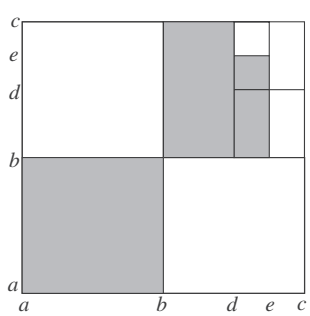

Fig. 5 Illustration of subpavings.

A. Interval Analysis and μ Analysis for Linear Clearance

To perform linear clearance, another known analysis method for stability margin calculation is μ analysis, first introduced in [23,24]. The structured singular value μ can be used to determine the stability of systems with uncertainty. The number μ is inversely proportional to the norm of perturbations that will cause singularity in the system, that is, the so-called worst-case perturbations. It is not possible to compute the number μ for a particular system; instead, an approximation is made by computing its upper and lower bounds. When these bounds are tight, the approximation is accurate.

In systems with real parametric uncertainties, the number μ is called the real structured singular value. The real μ is hard to approximate, and the computational effort for calculating the bounds is generally an exponential function of the size of the problem. To obtain a good approximation on μ, its tighter upper and lower bounds have to be obtained. The algorithm used to compute the bounds of real μ is not yet mature; a lot of research has been conducted on the computation of these bounds (see [25–30]).

The μ analysis is similar to interval analysis for linear clearance. The difference between the two techniques is that μ analysis only concerns the worst-case perturbations in the system, whereas interval analysis sweeps the whole system and looks for stable as well as unstable regions. Juliana et al. in [31,32] give an example of clearance for a system with real parametric uncertainties using the methods of μ analysis and interval analysis. The example shows that μ analysis alone gives only positive results, that is, the stable parameters in the system, without indicating the possible combinations of parameter that cause instability in the system. Interval analysis locates the unstable parameter combinations accurately, at the cost of high computational power. By combining the two methods, a tradeoff can be made between computational tractability and accuracy of the results.

B. Application of Algorithm for Nonlinear System Clearance

For the system model in Eq. (4), the stability domain $\mathbb{S}_P$ given by Eq. (9) can be obtained using the SIVIA algorithm. As explained in the previous section, the system contains uncertain parameter θ and time varying state x. Take the nominal value of the parameter θ as

$$\theta_0 = 0.5 \tag{19}$$

and the uncertainty bound as

$$\delta_\theta \in [-0.10, 0.10] \tag{20}$$

The system state is bounded by the interval

$$x \in [-0.6, 0.6] \tag{21}$$

Therefore, we obtain for this system a set of models in which the parameters vary within the intervals given by Eqs. (20) and (21).

The SIVIA algorithm performs the inverse mapping in Eq. (9) to obtain the stability domain $\mathbb{S}_P$. The algorithm starts with an evaluation of the whole set and does interval bisections for the cases in which the solutions are undetermined. The result is shown in Fig. 6. The figure shows the parameter space of the system, which is divided into two regions. The shaded region is the stable domain $\mathbb{S}_P$, whereas outside the shaded region the system is not cleared. The lines within the shaded region show the bisections of the interval. For the cleared region, the derivative of the Lyapunov function in Eq. (7) is negative semidefinite. We perform the clearance for this system using the interval toolbox in a MATLAB® environment. The calculation needs 7033 iterations to perform parameter interval bisections.

Because the Lyapunov function gives sufficient condition of stability, we can guarantee that the shaded area in Fig. 6 is stable. However, the stability condition in the region outside the shaded area is not known. For this region we can find other candidates of Lyapunov functions, or we can combine the analysis with simulations of the nonlinear model, in which we examine the critical region outside the stable area. The combination of the analysis and the simulations will reduce the conservatism in the result.

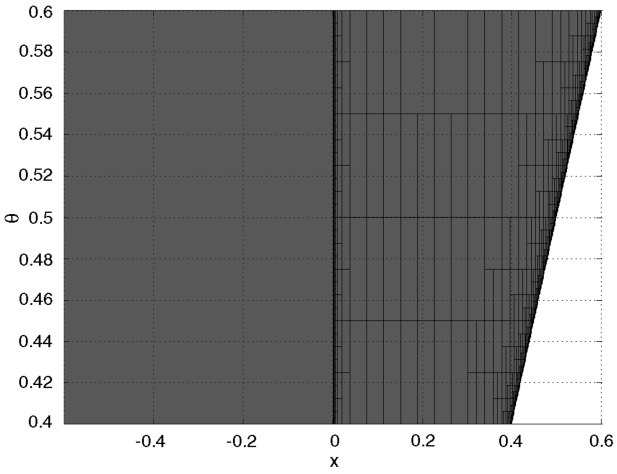

Fig. 6 The clearance result in the parameter space θ vs x; the shaded area is cleared.

This example gives a picture on how clearance can be performed on nonlinear systems using interval analysis. In the next section, the method is applied to reentry flight clearance, in which linear and nonlinear models of a reentry vehicle are investigated.

VI. Clearance of Delft Aerospace Reentry Test Vehicle

This section presents the case study of reentry flight clearance performed on a reentry vehicle flight control system. The reentry vehicle is called the Delft Aerospace Reentry Test (DART) demonstrator. The DART reentry vehicle is a double-cone capsule with 1.36 m of length, 0.67 m of base radius, and 137 kg of weight. Figure 7 shows the shape of the capsule.

The goal of the DART project is to develop, build, and fly a small, reusable, low-cost reentry test bed for the purpose of fundamental studies of selected topics concerning reentry. The mission scenario of the DART reentry flight is as follows. The vehicle is carried as a payload in a rocket and launched from the Earth. After separation from its carrier in the outermost layer of the Earth's atmosphere, the vehicle has to perform the assigned

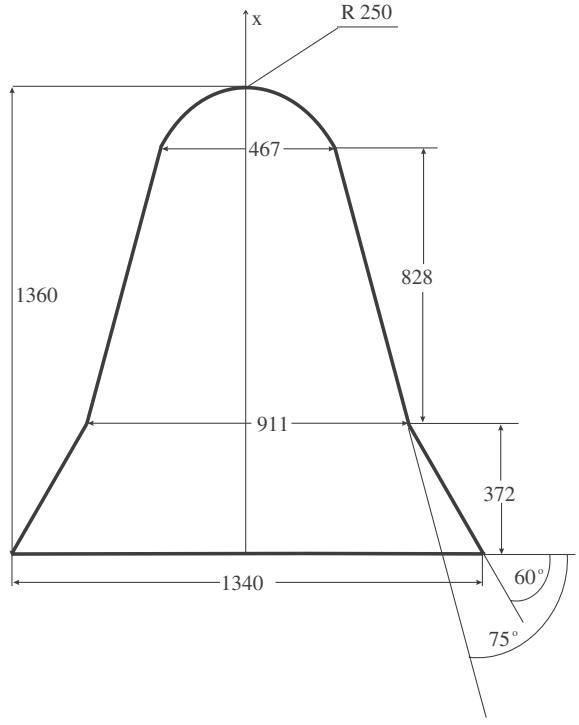

Fig. 7 The concept of DART: length unit in millimeters.

aerothermodynamic experiments during its reentry flight and returns back to Earth with the collected data [33].

The vehicle is equipped with a flight control system, which is responsible for maintaining a constant body spin rate and for keeping the aerodynamic attitude angles at the reference points. The control actuators are three pairs of cold gas thrusters located at the base of the vehicle. Because the dynamics of the system are highly nonlinear, nonlinear control laws are more suitable for this system. The nonlinear dynamic inversion (NDI) technique, combined with the linear proportional integral derivative (PID) technique, is applied as the feedback control for the vehicle.

The scenario of the DART control system is defined as follows [33]. When separated from the launcher, the vehicle is spun about its body X_B axis with an angular velocity of 20 deg/s, which is maintained constant by the controller. The purpose of the spinning motion is to provide the vehicle with gyroscopic rigidity. Besides the spinning, active control is employed to reduce the coning motion and make the aerodynamic angles α and β close to zero. The control system is active until the vehicle reduces its speed to a Mach number of $M = 2$, at which a set of parachutes is deployed to further decelerate the vehicle until it reaches the intended landing spot.

A. Mathematical Model

The NDI control law is responsible for linearizing the system in order to apply the PID technique in the outer loop. Figure 8 shows the block diagram of NDI and PID in two feedback loops. NDI uses the inversion of the system dynamics to perform feedback linearization. To get a perfect linearized system, one has to have a perfect model of the original system. If the model of the system contains uncertainty, the system cannot be completely linearized [34]. It is assumed that the mathematical model of DART contains uncertainty in parameters. The model of the closed-loop system is, therefore, still nonlinear and contains the uncertain parameters.

The model of the closed-loop system can be expressed in general form as

$$\dot{x} = f(x, P) \tag{22}$$

with x the states, P the constant or varying parameters, and f the nonlinear functions of the states and the parameters. The system under consideration concerns the rotational motion of the vehicle. Therefore, the states of the dynamic model consist of the angular rates and the aerodynamic angles. The translational motion parameters, which are the translational position and velocity vectors, are considered as varying parameters in vector P. The parameter vector P also contains the inertia properties, the controller gains, the atmospheric properties, and the uncertainty in the aerodynamic moments.

In the following example, the model of the DART control system in the presence of parametric uncertainty is constructed. The uncertainty is assumed to originate mainly from aerodynamic modeling error. As a consequence of the error, the closed-loop system model becomes more complex with the existence of some nonlinear terms. These terms are functions of the differences between the real and the modeled aerodynamic moments. In the model construction, the magnitude of the aerodynamic moments is assumed to be uncertain, with the uncertainty assumed to be bounded.

The control system model with these nonlinear terms can be expressed as

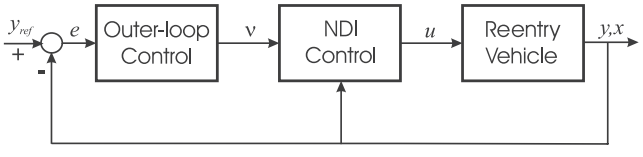

Fig. 8 Feedback control system with nonlinear dynamic inversion.

$$\begin{bmatrix} \dot{p} \\ \ddot{\alpha} \\ \ddot{\beta} \end{bmatrix} = \begin{bmatrix} \nu_1 \\ \nu_2 \\ \nu_3 \end{bmatrix} + \begin{bmatrix} \frac{1}{I_{xx}} & 0 & 0 \\ \frac{-\cos\alpha\tan\beta}{I_{yy}} & \frac{1}{I_{yy}} & \frac{-\sin\alpha\tan\beta}{I_{yy}} \\ \frac{\sin\alpha}{I_{zz}} & 0 & \frac{-\cos\alpha}{I_{zz}} \end{bmatrix} [M_A - \tilde{M}_A] \tag{23}$$

In the outer feedback loop, the control inputs $\nu = [\,\nu_1 \quad \nu_2 \quad \nu_3\,]^T$ are designed with the PID technique as

$$\nu_1 = \left(K_{P1} + \frac{K_{I1}}{s}\right) e_p \tag{24}$$

$$\nu_2 = (K_{P2} + K_{D2}s) e_\alpha \tag{25}$$

$$\nu_3 = (K_{P3} + K_{D3}s) e_\beta \tag{26}$$

where the terms K_P, K_I, and K_D are the proportional, integral, and derivative gains, respectively. The controlled variables are the differences between the references and the outputs, that is,

$$\begin{bmatrix} e_p \\ e_\alpha \\ e_\beta \end{bmatrix} = \begin{bmatrix} p_{\text{ref}} - p \\ \alpha_{\text{ref}} - \alpha \\ \beta_{\text{ref}} - \beta \end{bmatrix} \tag{27}$$

The aerodynamic moments are assumed to contain uncertainties; they can be expressed as

$$M_A = (I_{3\times3} + \Delta_{M_A}) \cdot \tilde{M}_A \tag{28}$$

where $I_{3\times3}$ is a 3-by-3 identity matrix, and

$$\Delta_{M_A} = \begin{bmatrix} \delta_{M_{Ax}} & 0 & 0 \\ 0 & \delta_{M_{Ay}} & 0 \\ 0 & 0 & \delta_{M_{Az}} \end{bmatrix}; \qquad M_A = [\,M_{Ax} \quad M_{Ay} \quad M_{Az}\,]^T;$$
$$\tilde{M}_A = [\,\tilde{M}_{Ax} \quad \tilde{M}_{Ay} \quad \tilde{M}_{Az}\,]^T$$

in which $\delta_{M_{Ax}}$, $\delta_{M_{Ay}}$, and $\delta_{M_{Az}}$ are aerodynamic uncertainties. Substituting Eq. (28) into Eq. (23), we obtain

$$\begin{bmatrix} \dot{p} \\ \ddot{\alpha} \\ \ddot{\beta} \end{bmatrix} = \begin{bmatrix} \nu_1 \\ \nu_2 \\ \nu_3 \end{bmatrix} + \frac{1}{\cos\beta} \begin{bmatrix} \cos\beta & 0 & 0 \\ -\cos\alpha\sin\beta & \cos\beta & -\sin\alpha\sin\beta \\ \sin\alpha\cos\beta & 0 & -\cos\alpha\cos\beta \end{bmatrix} \begin{bmatrix} \frac{\delta_{M_{Ax}}\tilde{M}_{Ax}}{I_{xx}} \\ \frac{\delta_{M_{Ay}}\tilde{M}_{Ay}}{I_{yy}} \\ \frac{\delta_{M_{Az}}\tilde{M}_{Az}}{I_{zz}} \end{bmatrix} \tag{29}$$

The values of the uncertainty parameters $\delta_{M_{Ax}}$, $\delta_{M_{Ay}}$, and $\delta_{M_{Az}}$ are unknown but assumed to be bounded. These bounds represent the relative magnitude of these parameters with respect to the predicted aerodynamic moments. This can be illustrated by taking any element from Eq. (28), for example,

$$M_{Ax} = \tilde{M}_{Ax}(1 + \delta_{M_{Ax}}) \tag{30}$$

In Eq. (30), the true moment M_{Ax} is equal to the nominal value of $\tilde{M}_{Ax}$ if $\delta_{M_{Ax}} = 0$. Otherwise, as $\delta_{M_{Ax}} \neq 0$, the magnitude of M_{Ax} will be larger or smaller relative to the predicted aerodynamic moment $\tilde{M}_{Ax}$.

The clearance of DART reentry flight aims to evaluate the stability of the vehicle within its flight region in the presence of the uncertain parameters in the model. The state space and the parameter space have to be cleared according to the chosen stability criteria. As a result of the clearance, the vehicle is certified as stable in the cleared region.

Table 2 shows the division of the DART reentry flight envelope for the clearance purpose. The table shows segments of the Mach number and altitude, which are two varying parameters during reentry flight. These regions are defined around the nominal reentry flight trajectory.

Table 2 Division of the DART reentry flight envelope for the clearance

Segment	Mach	Altitude, km	Segment	Mach	Altitude, km
1	[24, 26]	[78, 96]	13	[5.5, 6.5]	[30.3, 31.4]
2	[22, 24]	[64, 78]	14	[4.7, 5.5]	[29.4, 30.4]
3	[20, 22]	[55, 65]	15	[4.3, 4.7]	[28.9, 29.5]
4	[18, 20]	[48, 56]	16	[3.9, 4.3]	[28.3, 28.9]
5	[16, 18]	[42, 49]	17	[3.5, 3.9]	[27.6, 28.3]
6	[14, 16]	[39, 43]	18	[3.3, 3.5]	[27.2, 27.7]
7	[12, 14]	[36.5, 39.5]	19	[3.1, 3.3]	[26.9, 27.3]
8	[10.5, 12]	[35.2, 37]	20	[2.9, 3.1]	[26.5, 27]
9	[9.5, 10.5]	[34.2, 35.3]	21	[2.7, 2.9]	[26.1, 26.6]
10	[8.5, 9.5]	[33.2, 34.3]	22	[2.5, 2.7]	[25.6, 26.2]
11	[7.5, 8.5]	[32.3, 33.3]	23	[2.3, 2.5]	[25.2, 25.7]
12	[6.5, 7.5]	[31.3, 32.4]	24	[2.1, 2.3]	[24.7, 25.3]

For each segment, a nonlinear model is constructed. The parameters in the models are different from one segment to another because the atmospheric parameters vary rapidly. As these models are cleared, the clearance process can be extended to other segments in the envelope such that all the possible flyable regions are covered.

B. Clearance Criteria for Delft Aerospace Reentry Test Vehicle

The clearance requirement for DART is stability in the flight domain in the presence of the parametric uncertainties. Two types of stability are examined: linear and nonlinear cases.

1. *Linear Clearance*

For a linear system, stability can be determined by evaluating the eigenvalues of the linear system. When the eigenvalues are in the left half of the complex plane, the system is stable.

The Routh–Hurwitz stability criterion can be used to look for the worst-case eigenvalues of a linear system. A necessary condition of stability for a linear system is when all the coefficients of the characteristic polynomial have the same sign. Take a linear system whose characteristic polynomial is of nth order, that is,

$$a_n\lambda^n + a_{n-1}\lambda^{n-1} + \cdots + a_0 = 0 \tag{31}$$

where λ is the eigenvalues of the system and $a_0, \ldots, a_n$ are the coefficients of the characteristic polynomial. To evaluate the necessary and sufficient condition of stability for this system, one can construct a so-called Routh table with the following rules. For an nth-order polynomial, if n is an even number, the first and second rows of the array can be constructed as in Table 3. The third up to $n + 1$ rows follow the rules shown in Table 4.

The Routh–Hurwitz stability criterion states that all the coefficients in the first column of the table must be positive for the roots of the polynomial in Eq. (31) to be in the left half of the complex plane. These coefficients are functions of the parameters in the original linear system. We denote this parameter set as $P \in \mathbb{R}^{n_P}$. When the values of these parameters are not constant, but varying within some intervals, the evaluation of the coefficients can be performed with interval analysis.

The stability domain is mapped using the Routh–Hurwitz stability criteria onto the positive real line. The coefficients in the first column of the Routh table have to be positive for the linear system to be stable. Therefore, the stability domain of the linear system can be defined as

$$\mathbb{S}_P \equiv \{P \in \mathbb{R}^{n_P} | \mathbf{r}(P) > 0\} = \mathbf{r}^{-1}(]0, +\infty[^{\times n}) \tag{32}$$

where the vector function $\mathbf{r}$ is defined from the first column of the Routh table.

Table 3 The first- and second-row elements of the Routh table

Row 1	a_n	a_{n-2}	...	a_0
Row 2	a_{n-1}	a_{n-3}	...	0

From Eq. (32), the stability domain can be obtained by finding the inverse mapping of $\mathbf{r}$ into the parameter space $\mathbb{R}^{n_P}$. The characterization of the stability domain $\mathbb{S}_P$ as defined by Eq. (32) can thus be cast into the framework of set inversion given by Eq. (13) and performed by the SIVIA algorithm.

2. *Nonlinear Clearance*

For a nonlinear system, the stability can be determined by the Lyapunov theorem. Consider a general nonlinear autonomous system model, which can be written as in Eq. (22). In the model, f is a nonlinear continuous function. The system is autonomous, as the function f does not depend explicitly on time.

For this system, construct a positive–definite function

$$V(x, P):\mathbb{R}^n \to \mathbb{R}, \qquad V(x, P) > 0 \tag{33}$$

which has continuous partial derivatives in the neighborhood of the equilibria. If its time derivative along any state trajectory of the system in Eq. (22) is negative semidefinite, that is,

$$\dot{V}(x, P) \leq 0 \tag{34}$$

then $V(x, P)$ is called the Lyapunov function for the system in Eq. (22).

The condition given in Eqs. (33) and (34) seems to severely limit the scope of the analysis only to ideal continuous systems. However, in the case that the system has discontinuities, for instance in the slope of atmosphere properties vs altitude, one can divide the model at the discontinuity point such that one can obtain several models that still behave as continuous systems. In the cases of discontinuities in aerodynamic models, the same strategy can also be applied. This makes the analysis become a hybrid between continuous and discrete/grid-point approach.

The Lyapunov theorem for local stability is defined by Eqs. (33) and (34) [35]. When the time derivative of a positive–definite Lyapunov function is negative semidefinite, the system is said to be locally stable. When this derivative is negative definite, the system is said to be locally asymptotically stable. For global stability, one has to consider the whole state space instead of the neighborhood of the equilibria. Moreover, the Lyapunov function $V(x, P)$ has to be radially unbounded.

The existence of a Lyapunov function for the system in Eq. (22) provides sufficient condition for stability in the system. We are interested to know the stable part of the state and parameter space of this system, which we call the stability domain, denoted as $\mathbb{S}_P$. When the states x and the parameters P are varying, the problem of finding the stability domain can be solved using interval analysis as follows.

Table 4 The third until $n + 1$ row elements of the Routh table

	Column 1		Column i	Column $i + 1$
Row k-2	x_1	$\cdots$		x_{i+1}
Row k-1	y_1	$\cdots$		y_{i+1}
Row k	z_1	$\cdots$	$z_i = \frac{1}{y_1} \cdot (y_1 x_{i+1} - y_{i+1} x_1)$	

In the first instance we take a candidate of the Lyapunov function V for the system, which for a mechanical system can be a scalar energy function. This function has to be positive definite. The candidate is probably a function of the varying states and parameters. Then we find the first-order derivative of this function, $\dot{V}$, which may still contain the states and the parameters. This derivative has to be negative semidefinite for the system to be stable. It means that the function $\dot{V}$ has to map the domain of the states and parameters into the negative real line including zero for the system to be stable. Therefore, to obtain the stability domain, we have to find the inverse mapping of the scalar function $\dot{V}$, that is,

$$\mathbb{S}_P \equiv \{(x, P) \in \mathbb{R}^n | \dot{V}(P) \leq 0\} = \dot{V}^{-1}(]-\infty, 0]) \tag{35}$$

Using Eq. (35), the characterization of the stability domain $\mathbb{S}_P$ can thus be cast into the framework of set inversion given by Eq. (13) and performed by the SIVIA algorithm.

C. Numerical Results

For the DART reentry flight clearance, two stability criteria are evaluated using the SIVIA algorithm, that is, the linear and nonlinear criteria. In the linear clearance, worst-case eigenvalues are evaluated, whereas in the nonlinear clearance, the Lyapunov function of the closed-loop system is evaluated. The clearance results determine the stability robustness of the control system within the flying regime of the vehicle. Both linear and nonlinear clearance results are presented and compared in the following.

Note: There is one singularity in the system, namely the origin itself. To understand this singularity, the concept of total angle of attack is introduced here. This is a combination of the commonly known angle of attack α and sideslip angle β. This concept can be seen in Fig. 9. From the velocity vector V and the X_B axis in body reference frame, a plane is created. This is called the windward meridian plane, that is, the plane $O - X_B - V - V''$ in the figure.

The angle between the velocity vector V and X_B axis is called the total angle of attack τ, because it is a combination of angle of attack α and sideslip angle β, as shown in Fig. 9. This angle can be defined as

$$\tau = \cos^{-1}(\cos\alpha \cos\beta) \tag{36}$$

Furthermore, the windward meridian plane forms an angle with the Z_B vector, which can be calculated as

$$\zeta = \sin^{-1} \frac{\cos\alpha \sin\beta}{\sqrt{1 - (\cos\alpha \cos\beta)^2}} \tag{37}$$

These two angles are used to calculate the components of aerodynamic forces and moments in body reference frame for the DART aerodynamic model.

The angle ζ given by Eq. (37) is undefined for $\alpha = 0$ and $\beta = 0$. Because it is undefined, the calculation at this point will cause a singularity problem. Despite the singularity, this point is the equilibrium point, which is known to be stable from the nominal analysis. Therefore, the point can be excluded safely from the evaluation.

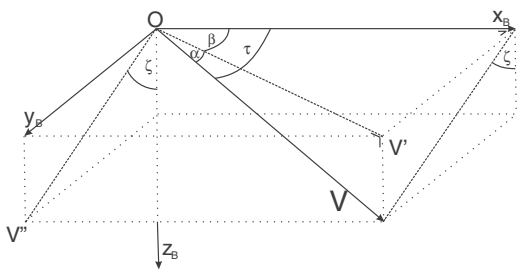

Fig. 9 Geometric scheme of windward meridian plane.

1. Linear Clearance

The model of the DART control system with aerodynamic parameter uncertainties as shown in Eq. (29) is nonlinear; therefore, it first has to be linearized to make the linear clearance tool applicable. The linearization takes place on the reference points p_{ref}, α_{ref}, and β_{ref} in the nominal flight conditions. Rewrite Eq. (29) as

$$\begin{bmatrix} \dot{p} \\ \ddot{\alpha} \\ \ddot{\beta} \end{bmatrix} = \begin{bmatrix} f_{\dot{p}} \\ f_{\ddot{\alpha}} \\ f_{\ddot{\beta}} \end{bmatrix} + \begin{bmatrix} \nu_1 \\ \nu_2 \\ \nu_3 \end{bmatrix} \tag{38}$$

where the functions $f_{\dot{p}}$, $f_{\ddot{\alpha}}$, and $f_{\ddot{\beta}}$ are defined as

$$f_{\dot{p}} = \frac{\delta_{M_{Ax}} \tilde{M}_{Ax}}{I_{xx}} \tag{39}$$

$$f_{\ddot{\alpha}} = -\frac{\delta_{M_{Ax}} \tilde{M}_{Ax}}{I_{xx}} \cos\alpha \tan\beta + \frac{\delta_{M_{Ay}} \tilde{M}_{Ay}}{I_{yy}} - \frac{\delta_{M_{Az}} \tilde{M}_{Az}}{I_{zz}} \sin\alpha \tan\beta \tag{40}$$

$$f_{\ddot{\beta}} = \frac{M_{Ax} - \tilde{M}_{Ax}}{I_{xx}} \sin\alpha + \frac{\tilde{M}_{Az} - M_{Az}}{I_{zz}} \cos\alpha \tag{41}$$

The state variables are

$$x = [\,\hat{p} \quad p \quad \alpha \quad \dot{\alpha} \quad \beta \quad \dot{\beta}\,]^T$$

where we introduce the state variable $\hat{p}$, which represents the time integrated roll rate p, such that

$$\frac{\partial \hat{p}}{\partial t} = \dot{\hat{p}} = p \tag{42}$$

From the nonlinear model, the linearized NDI control system with uncertainties can be constructed using the first-order Taylor expansion. It can be written in state-space form as

$$\dot{x} = A_{\text{ol}} x + B_{\text{ol}} \nu = \begin{bmatrix} 0 & 1 & 0 & 0 & 0 & 0 \\ 0 & 0 & a & 0 & b & 0 \\ 0 & 0 & 0 & 1 & 0 & 0 \\ 0 & 0 & c & 0 & d & 0 \\ 0 & 0 & 0 & 0 & 0 & 1 \\ 0 & 0 & e & 0 & f & 0 \end{bmatrix} x + \begin{bmatrix} 0 & 0 & 0 \\ 1 & 0 & 0 \\ 0 & 0 & 0 \\ 0 & 1 & 0 \\ 0 & 0 & 0 \\ 0 & 0 & 1 \end{bmatrix} \nu + \begin{bmatrix} 0 \\ g \\ 0 \\ h \\ 0 \\ k \end{bmatrix} \tag{43}$$

where the terms

$$a = \left.\frac{\partial f_{\dot{p}}}{\partial \alpha}\right|_{\alpha_0,\beta_0}, \quad b = \left.\frac{\partial f_{\dot{p}}}{\partial \beta}\right|_{\alpha_0,\beta_0}, \quad c = \left.\frac{\partial f_{\ddot{\alpha}}}{\partial \alpha}\right|_{\alpha_0,\beta_0},$$
$$d = \left.\frac{\partial f_{\ddot{\alpha}}}{\partial \beta}\right|_{\alpha_0,\beta_0}, \quad e = \left.\frac{\partial f_{\ddot{\beta}}}{\partial \alpha}\right|_{\alpha_0,\beta_0}, \quad f = \left.\frac{\partial f_{\ddot{\beta}}}{\partial \beta}\right|_{\alpha_0,\beta_0}$$

$g = f_{\dot{p}}(0)$, $h = f_{\ddot{\alpha}}(0)$, and $k = f_{\ddot{\beta}}(0)$. To calculate the partial derivatives that define the terms a, b, c, d, e, and f, the expressions for the aerodynamic moments M_{Ax}, M_{Ay}, and M_{Az} are needed. These can be found in the Appendix.

By applying the PID control law in the outer loop, the closed-loop system is obtained. The system can be expressed as

$$\dot{x} = A_{\text{cl}}x + B_{\text{cl}}x_{\text{ref}} \tag{44}$$

where x_{ref} is the reference values of the state variables. The second term in the equation is constant and, therefore, does not have to be included in the stability analysis. The clearance is performed by evaluating the closed-loop system matrix A_{cl}, which can be written as

$$\begin{bmatrix} 0 & 1 & 0 & 0 & 0 & 0 \\ -K_{I1} & -K_{P1} & a & 0 & b & 0 \\ 0 & 0 & 0 & 1 & 0 & 0 \\ 0 & 0 & c - K_{P2} & -K_{D2} & d & 0 \\ 0 & 0 & 0 & 0 & 0 & 1 \\ 0 & 0 & e & 0 & f - K_{P3} & -K_{D3} \end{bmatrix} \tag{45}$$

which contains the controller gains and the nonlinear terms a, b, c, d, e, and f. The latter are functions of the uncertainties $\delta_{M_{Ax}}$, $\delta_{M_{Ay}}$, and $\delta_{M_{Az}}$ and the flight conditions.

For the linear clearance, each segment within the DART reentry flight envelope, shown in Table 2, cannot be evaluated simultaneously. The linear model is valid only locally around discrete points within the flight envelope. Therefore, to apply the linear clearance, the trajectory has to be divided into many points.

The SIVIA algorithm evaluates the characteristic polynomial of the closed-loop system, constructed from the determinant of the closed-loop system matrix A_{cl}, which contains the uncertain parameters. The characteristic polynomial of the DART linearized control system can be written as

$$P(s) = a_6 s^6 + a_5 s^5 + a_4 s^4 + a_3 s^3 + a_2 s^2 + a_1 s + a_0 \tag{46}$$

where the coefficients $a_0, \ldots, a_6$ are functions of the uncertain parameters. From Eq. (46), the Routh table can be constructed as in Tables 3 and 4. The calculation of the coefficients of the characteristic polynomials in Eq. (46) is done using the symbolic toolbox of MATLAB.

For one point at Mach number $M = 12.1$ and altitude 37.0 km, the coefficients of the characteristic polynomial $P(s)$ can be written as

$$\left.\begin{aligned} a_6 &= 1, \\ a_5 &= 10.9, \\ a_4 &= 67.9 + 6.7 \times 10^{-9}\delta_{M_{Ax}} + 746.0(\delta_{M_{Ay}} + \delta_{M_{Az}}), \\ a_3 &= 258.8 + 4.3 \times 10^{-8}\delta_{M_{Ax}} + 4827.9(\delta_{M_{Ay}} + \delta_{M_{Az}}), \\ a_2 &= 678.8 + 1.9 \times 10^{-7}\delta_{M_{Ax}} + 21592(\delta_{M_{Ay}} + \delta_{M_{Az}}) + 4.9 \times 10^{-4}\delta_{M_{Ax}}\delta_{M_{Ay}} \\ &\quad + 5.5 \times 10^{5}\delta_{M_{Ay}}\delta_{M_{Az}} - 5.1 \times 10^{-4}\delta_{M_{Ax}}\delta_{M_{Az}} + 4.8 \times 10^{-6}\delta_{M_{Ax}}^2 + 1.7\delta_{M_{Az}}^2, \\ a_1 &= 1094.3 + 4.3 \times 10^{-7}\delta_{M_{Ax}} + 48279(\delta_{M_{Ay}} + \delta_{M_{Az}}) + 9.9 \times 10^{-4}\delta_{M_{Ax}}\delta_{M_{Ay}} \\ &\quad + 1.1 \times 10^{6}\delta_{M_{Ay}}\delta_{M_{Az}} - 1 \times 10^{-3}\delta_{M_{Ax}}\delta_{M_{Az}} + 9.6 \times 10^{-6}\delta_{M_{Ax}}^2 + 3.4\delta_{M_{Az}}^2, \\ a_0 &= 1000 + 6.7 \times 10^{-7}\delta_{M_{Ax}} + 74602(\delta_{M_{Ay}} + \delta_{M_{Az}}) + 5 \times 10^{-3}\delta_{M_{Ax}}\delta_{M_{Ay}} \\ &\quad + 5.6 \times 10^{6}\delta_{M_{Ay}}\delta_{M_{Az}} - 5.1 \times 10^{-3}\delta_{M_{Ax}}\delta_{M_{Az}} + 4.8 \times 10^{-5}\delta_{M_{Ax}}^2 + 16.9\delta_{M_{Az}}^2, \end{aligned}\right\} \tag{47}$$

in which the uncertain parameters may vary within the intervals given in Table 5.

The necessary and sufficient condition for linear system stability is that all the terms in the first column of the Routh table, constructed from the coefficients of the characteristic equations, are positive. As these conditions are fulfilled, the eigenvalues of the closed-loop system are in the left half of the complex plane; therefore, the closed-loop system is stable.

Table 5 The DART flight conditions for $M = 12.1$ and $h = 37.0$ km for linear clearance

State	Value	Parameter	Value
α	0.1 deg	V	3774 m/s
β	0.1 deg	ρ	6.2×10^{-3} kg m^{-3}
p	20 deg/s	$\delta_{M_{Ax}}$	[−0.05, 0.05]
q	0 deg/s	$\delta_{M_{Ay}}$	[−0.05, 0.05]
r	0 deg/s	$\delta_{M_{Az}}$	[−0.05, 0.05]

The clearance result for the linearized model at Mach number $M = 12.1$ and altitude 37.0 km is presented in Fig. 10. The figure shows a two-dimensional parameter space of $\delta_{M_{Ay}}$ and $\delta_{M_{Az}}$, which are two of the aerodynamic uncertainties in the system. The shaded region in the figure is the cleared parameter space, that is, the intervals for which the system is stable. The set of states and parameters in the model for Fig. 10 are shown in Table 5. The system is cleared in the reference points, in the presence of the uncertain parameters $\delta_{M_{Ax}}$, $\delta_{M_{Ay}}$, and $\delta_{M_{Az}}$. For this point, the uncertainty $\delta_{M_{Ax}}$ does not influence the system stability. Therefore, Fig. 10 only shows the parameters $\delta_{M_{Ay}}$ and $\delta_{M_{Az}}$, because their values affect the stable and unstable regions in the system. For this calculation, the algorithm iterates 8543 times, which is equal to the number of interval bisections.

The clearance result shows that the system is stable in the nominal flight condition and within the shaded area in Fig. 10. When the magnitude of the uncertainty in the model exceeds the boundary of the shaded region in Fig. 10, the system is no longer cleared. The result will be compared with the one from the nonlinear clearance.

Summarizing, the linear clearance for DART is performed as follows:

1) Linearize the nonlinear model at the investigated flight condition.

2) Construct the characteristic equation of the linearized model that is possibly a function of uncertainty.

3) Perform the clearance using the SIVIA algorithm by evaluating the Routh–Hurwitz stability criterion.

4) Distinguish the cleared subsystems from the noncleared ones.

5) Repeat the procedure for other flight conditions until all points are cleared.

2. *Nonlinear Clearance*

The nonlinear clearance of DART corresponds to analyzing the derivative of the positive–definite Lyapunov functions for the

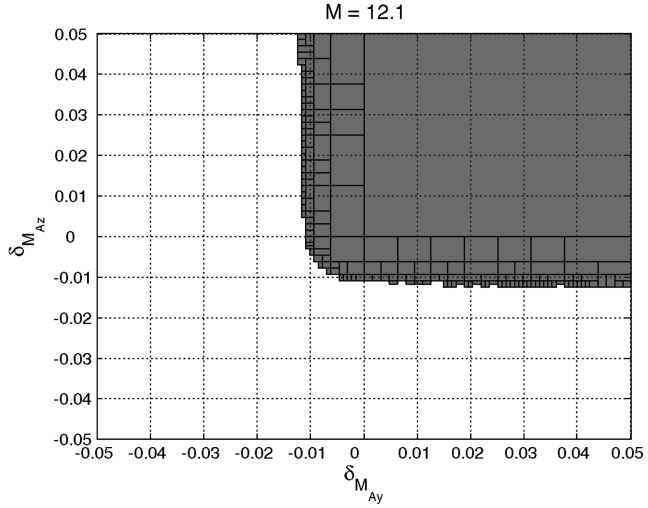

Fig. 10 DART linear clearance result for $M = 12.1$ and $h = 37.0$ km.

nonlinear system in Eq. (29). Although constructing a Lyapunov function is not a trivial task, for mechanical systems it is possible by using the energy dissipation principle. It stems from the fact that stable systems dissipate energy. Therefore, if there is a positive energy function for a system, this system is stable if the time derivative of this function is negative or zero. This implies that the energy is not accumulated in the system.

We may simplify the form of the closed-loop system by defining a new state vector:

$$\dot{q} = \frac{\partial q}{\partial t} = [\, p \quad \dot{\alpha} \quad \dot{\beta}\,]^T \tag{48}$$

We define two positive–definite matrices K_{I} and K_{II} that contain the PID controller gains, that is,

$$K_{\mathrm{I}} = \begin{bmatrix} K_{P1} & 0 & 0 \\ 0 & K_{D2} & 0 \\ 0 & 0 & K_{D3} \end{bmatrix} \tag{49}$$

and

$$K_{\mathrm{II}} = \begin{bmatrix} K_{I1} & 0 & 0 \\ 0 & K_{P2} & 0 \\ 0 & 0 & K_{P3} \end{bmatrix} \tag{50}$$

Taking the notations from Eqs. (48–50) and removing the static terms from the model, we can rewrite the dynamics of the closed-loop system with aerodynamic moment uncertainties as

$$\ddot{q} = -K_{\mathrm{I}}\dot{q} - K_{\mathrm{II}}q + AI_n^{-1}\Delta_{M_A}\tilde{M}_A \tag{51}$$

with

$$A = \begin{bmatrix} 1 & 0 & 0 \\ -\cos\alpha\tan\beta & 1 & -\sin\alpha\tan\beta \\ \sin\alpha & 0 & -\cos\alpha \end{bmatrix};$$

$$I_n^{-1} = \begin{bmatrix} \frac{1}{I_{xx}} & 0 & 0 \\ 0 & \frac{1}{I_{yy}} & 0 \\ 0 & 0 & \frac{1}{I_{zz}} \end{bmatrix}; \qquad \Delta_{M_A} = \begin{bmatrix} \delta_{M_{Ax}} & 0 & 0 \\ 0 & \delta_{M_{Ay}} & 0 \\ 0 & 0 & \delta_{M_{Az}} \end{bmatrix},$$

$$\tilde{M}_A = [\, \tilde{M}_{Ax} \quad \tilde{M}_{Ay} \quad \tilde{M}_{Az}\,]^T$$

where $\tilde{M}_A$ is the model of the aerodynamic moments, which are nonlinear functions of the states and the flight conditions.

A Lyapunov function can be constructed as the sum of the artificial kinetic and potential energy functions of the system. The artificial kinetic energy can be written as

$$E_k = \tfrac{1}{2}\dot{q}^T\dot{q} \tag{52}$$

which is a quadratic function of the body rate; and the artificial potential energy can be written as

$$E_p = \tfrac{1}{2}(q^T K_{\mathrm{II}} q) \tag{53}$$

The Lyapunov function is constructed as the summation of the kinetic and potential energy, that is,

$$V = \tfrac{1}{2}(\dot{q}^T\dot{q} + q^T K_{\mathrm{II}} q) \tag{54}$$

The Lyapunov function in Eq. (54) is positive semidefinite because it is quadratic and K_{II} is positive definite. To check the system stability, take the first-order derivative of the Lyapunov function, that is,

$$\dot{V} = \dot{q}^T\ddot{q} + \dot{q}^T K_{\mathrm{II}} q \tag{55}$$

For the closed-loop system with uncertainty, the first-order derivative of V can be written using Eqs. (51) and (55) as

$$\dot{V} = -\dot{q}^T K_{\mathrm{I}}\dot{q} + \dot{q}^T AI_n^{-1}\Delta_{M_A}\tilde{M}_A \tag{56}$$

in which values are functions of the flight conditions and states, as well as uncertain parameters in the DART flight envelope.

The model set of the control system is cleared if the function $\dot{V}$ is negative semidefinite for all the subsystems in the set. To know this, the variation of flight conditions and states, as well as the uncertainty, have to be applied to the closed-loop system to evaluate the stability. However, this evaluation gives a sufficient condition of stability. If $\dot{V}$ is not negative semidefinite in certain flight conditions and parameter combinations, the system is not necessarily unstable. In this case, we have to find another candidate of Lyapunov function.

Taking the variation of the flight conditions as well as the uncertain parameters into account, each segment in the flight envelope of DART can be evaluated as a continuous system. Besides the Mach number and altitude shown in Table 2, each segment also includes variation in the state variables, air density, velocity, and the uncertain aerodynamic parameters. In the clearance process, the states are allowed to vary around the equilibrium points within certain intervals. The intervals of the uncertainties are also assumed to be bounded, and the variations of the flight conditions for each segment are calculated for the range of the given Mach number and altitude.

The negative semidefiniteness of $\dot{V}$ in Eq. (55) is evaluated using the SIVIA algorithm. One result is presented in Fig. 11 for segment 7 in Table 2. The figure shows the parameter space $\delta_{M_{Ay}} - \delta_{M_{Az}}$, in which the shaded region represents stability of the system in the presence of the aerodynamic parameter uncertainties. Outside this region, the system is not guaranteed to be stable. The intervals of states and parameters for this segment are given in Table 6. For this

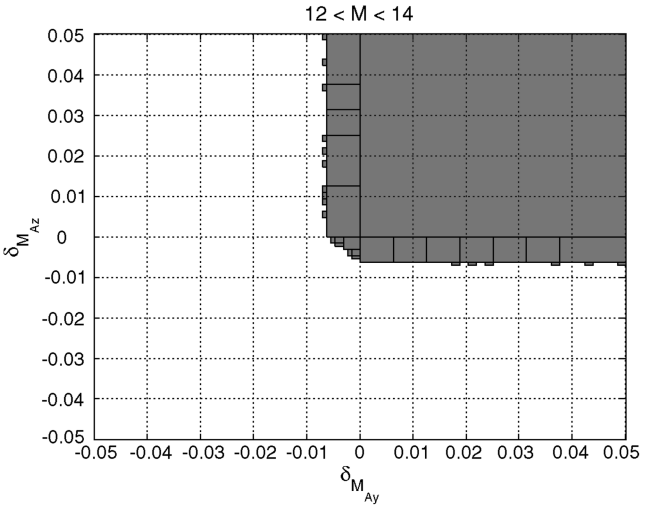

Fig. 11 DART nonlinear clearance result for segment 7 in Table 2.

Table 6 The DART flight conditions for segment 7 in Table 2

State	Value	Parameter	Value
α	$[-1,0)\cup(0,1]$ deg	V	[3624, 4456] m/s
β	$[-1,0)\cup(0,1]$ deg	ρ	$[4.26, 6.7]\times 10^{-3}$ kg m^{-3}
p	$[-1,1]$ deg/s	$\delta_{M_{Ax}}$	$[-0.05, 0.05]$
q	$[-5.6,0)\cup(0,5.6]$ deg/s	$\delta_{M_{Ay}}$	$[-0.05, 0.05]$
r	$[-5.6,0)\cup(0,5.6]$ deg/s	$\delta_{M_{Ax}}$	$[-0.05, 0.05]$

calculation, the algorithm iterates 45084 times, which is equal to the number of interval bisections.

The result is similar to the one from linear analysis (see Fig. 10). However, for the nonlinear clearance, the states and the parameters may vary within bounded intervals. Therefore, the result covers more area within the flight envelope of DART. A comparison of both methods in the next section provides more insight into the feasibility of the algorithm.

Summarizing, the nonlinear clearance for DART is performed as follows:

1) Define a positive–definite Lyapunov function for the nonlinear model.

2) Take the first-order derivative of the Lyapunov function, which is a function of the uncertain and varying parameters.

3) Perform the clearance using the SIVIA algorithm by checking in which subset the derivative of the Lyapunov function is negative semidefinite.

4) Distinguish the cleared subsystems from the noncleared ones.

5) When several nonlinear models are available, repeat the clearance for the other models.

3. *Comparison of the Results*

Compared with the result of the linear analysis, the Lyapunov function evaluation shows similar results. However, the destabilizing perturbation is smaller than the results given by the linear analysis. A comparative example can be presented for the linearized model at $M = 12.1$ and $h = 37.0$ km. To be able to compare the result, the nonlinear clearance with Lyapunov function analysis is also performed for this point. As a result, Fig. 12 shows the plots of the cleared uncertain parameters from the two methods: the Lyapunov function evaluation as the darker shaded area, and the eigenvalue analysis as the lighter shaded area. The discrepancy between the linear and nonlinear analyses is small and can be reduced by taking more bisection. However, the results agree on most of the cleared area.

To validate the result, a Monte Carlo analysis is performed on the linearized model at $M = 12.1$ and altitude $h = 37.0$ km. By varying the uncertain parameters on the linear model and sweeping the boundary in which the eigenvalues of the closed-loop system become unstable, we arrived at the result represented by the dots in Fig. 12. These are the points in the parameter space for which the closed-loop system is unstable. The results agree with both the linear and nonlinear interval analysis clearance.

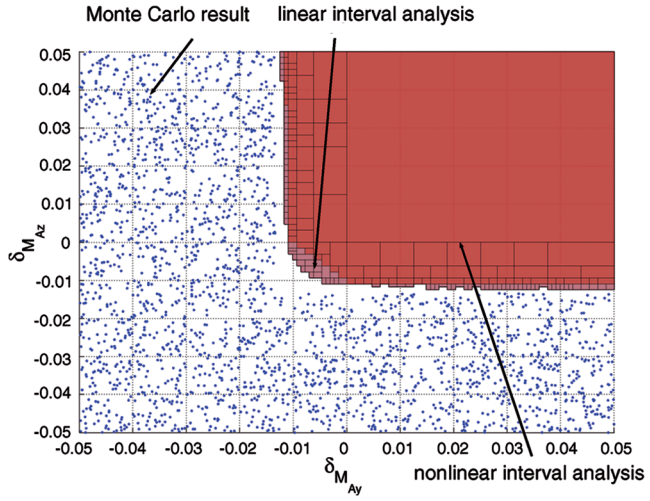

Fig. 12 Comparison of the DART clearance results from two methods.

VII. Conclusions

The approaches of linear and nonlinear clearance using interval analysis gave comparable results when applied to the case study. Additionally, Monte Carlo analysis confirmed the result of the clearance performed using interval analysis. Using both approaches in a complimentary fashion can deliver an advantage to the accuracy of the result as well as the computational effort. One can save the computational effort in Monte Carlo analysis by focusing on the critical region pointed out by interval analysis.

By implementing uncertainty bounds in the models, one can analyze the parameter space as a continuous system; hence, no single point in the parameter space is missed from the evaluation. The main advantage of interval analysis is that it can be applied directly to evaluate a model that was defined within certain bounds or intervals. The intervals may contain uncertain parameters, flight conditions, and the range of state variations, as shown in the nonlinear clearance of the reentry flight model. By doing this, important parameters can be represented simultaneously in one set of models.

As can be seen from the case study, only one type of uncertain parameters was considered. In reality, many sources of errors can be present in the model, which have to be addressed simultaneously. It is recommended that the applicability of the method is investigated for clearance of systems with a higher number of uncertain parameters. In doing so, one should be aware that the effect of an uncertain parameter to the system might be correlated to the effect of another parameter.

The order of the model used in the examples presented in this paper is relatively low. One should be aware that the computational load of the algorithm increases as a function of the number of uncertainties included in the model. To perform a large scale of clearance, which covers wider envelopes, various operating conditions, and numerous parametric uncertainties, a powerful computing machine will be needed.

Appendix: Approximation for Delft Aerospace Reentry Test Vehicle Aerodynamic Moments

The roll, pitch, and yaw aerodynamic moments of DART can be written as

$$M_{Ax} = \frac{1}{2}\rho V^2 SLC_{l_p}\frac{pL}{V}((1-f_{Kn})(1-f_{\text{bridge}})+f_{\text{bridge}}) \tag{A1}$$

$$\begin{aligned} M_{Ay} = \frac{1}{2}\rho V^2 SL\Bigg(& C_{m_q}\frac{qL}{V}((1-f_{Kn})(1-f_{\text{bridge}})+f_{\text{bridge}}) \\ & + \left(C_{m_{\text{hfm}}} + C_{z_{\text{hfm}}}\frac{x_{\text{cog}_{\text{hfm}}}}{L}\right) f_{Kn}(1-f_{\text{bridge}}) \\ & + \left(C_{m_{\text{hc}}} + C_{z_{\text{hc}}}\frac{x_{\text{cog}_{\text{hc}}}}{L}\right)(1-f_{Kn})(1-f_{\text{bridge}}) \\ & + \left(C_{m_s} + C_{z_s}\frac{x_{\text{cog}_s}}{L}\right) f_{\text{bridge}}\Bigg) \end{aligned} \tag{A2}$$

$$\begin{aligned} M_{Az} = \frac{1}{2}\rho V^2 SL\Bigg(& C_{n_r}\frac{rL}{V}((1-f_{Kn})(1-f_{\text{bridge}})+f_{\text{bridge}}) \\ & + \left(C_{n_{\text{hfm}}} - C_{y_{\text{hfm}}}\frac{x_{\text{cog}_{\text{hfm}}}}{L}\right) f_{Kn}(1-f_{\text{bridge}}) \\ & + \left(C_{n_{\text{hc}}} - C_{y_{\text{hc}}}\frac{x_{\text{cog}_{\text{hc}}}}{L}\right)(1-f_{Kn})(1-f_{\text{bridge}}) \\ & + \left(C_{n_s} - C_{y_s}\frac{x_{\text{cog}_s}}{L}\right) f_{\text{bridge}}\Bigg) \end{aligned} \tag{A3}$$

where $p \equiv$ roll rate, $q \equiv$ pitch rate, $r \equiv$ yaw rate, $\rho \equiv$ air density, $V \equiv$ airspeed, $S \equiv$ reference area, $L \equiv$ reference length, $x_{\text{cog}} \equiv x$ position of center of gravity with respect to moment reference point, f_{Kn} is a function of the Knudsen number, defined as

$$f_{Kn} = 0.5\left(1 + \frac{2}{\sqrt{\pi}} + \int_0^{(0.307\log(Kn)+0.806)} e^{-t^2}\,\mathrm{d}t\right) \tag{A4}$$

and f_{bridge} is a bridging function between hypersonic and supersonic regime, that is,

$$f_{\text{bridge}} = \begin{cases} 0, & \text{for } M > 5, \\ 5 - M, & \text{for } 4 \le M \le 5, \\ 1, & \text{for } M < 4 \end{cases} \tag{A5}$$

The aerodynamic coefficients C_{l_p}, C_{m_q}, and C_{n_r} are constant parameters, whereas the other aerodynamic coefficients are functions of flight conditions and aerodynamic angles. These approximation functions are made based on the aerodynamic database of DART. They are defined as

$$C_{m_{\text{hfm}}} = (C_{m_{\text{hfm0}}} + C_{m_{\text{hfm1}}}\tau + C_{m_{\text{hfm2}}}\tau^2 + C_{m_{\text{hfm3}}}\tau^3)\cos\zeta \tag{A6}$$

$$C_{m_{\text{hc}}} = (C_{m_{\text{hc0}}} + C_{m_{\text{hc1}}}\tau + C_{m_{\text{hc2}}}\tau^2 + C_{m_{\text{hc3}}}\tau^3)\cos\zeta \tag{A7}$$

$$C_{m_s} = -(C_{m_s0} + C_{m_s1}\tau)\cos\zeta \tag{A8}$$

$$C_{n_{\text{hfm}}} = -(C_{n_{\text{hfm0}}} + C_{n_{\text{hfm1}}}\tau + C_{n_{\text{hfm2}}}\tau^2 + C_{n_{\text{hfm3}}}\tau^3)\sin\zeta \tag{A9}$$

$$C_{n_{\text{hc}}} = -(C_{n_{\text{hc0}}} + C_{n_{\text{hc1}}}\tau + C_{n_{\text{hc2}}}\tau^2 + C_{n_{\text{hc3}}}\tau^3)\sin\zeta \tag{A10}$$

$$C_{n_s} = -(C_{n_s0} + C_{n_s1}\tau)\sin\zeta \tag{A11}$$

$$C_{y_{\text{hfm}}} = -(C_{y_{\text{hfm0}}} + C_{y_{\text{hfm1}}}\tau + C_{y_{\text{hfm2}}}\tau^2 + C_{y_{\text{hfm3}}}\tau^3)\sin\zeta \tag{A12}$$

$$C_{y_{\text{hc}}} = -(C_{y_{\text{hc0}}} + C_{y_{\text{hc1}}}\tau + C_{y_{\text{hc2}}}\tau^2 + C_{y_{\text{hc3}}}\tau^3)\sin\zeta \tag{A13}$$

$$C_{y_s} = -(C_{y_s0} + C_{y_s1}\tau)\sin\zeta \tag{A14}$$

$$C_{z_{\text{hfm}}} = -(C_{z_{\text{hfm0}}} + C_{z_{\text{hfm1}}}\tau + C_{z_{\text{hfm2}}}\tau^2 + C_{z_{\text{hfm3}}}\tau^3)\cos\zeta \tag{A15}$$

$$C_{z_{\text{hc}}} = -(C_{z_{\text{hc0}}} + C_{z_{\text{hc1}}}\tau + C_{z_{\text{hc2}}}\tau^2 + C_{z_{\text{hc3}}}\tau^3)\cos\zeta \tag{A16}$$

$$C_{z_s} = -(C_{z_s0} + C_{z_s1}\tau)\cos\zeta \tag{A17}$$

The subscript hfm stands for hypersonic free-molecular flow, hc stands for hypersonic continuum flow, and s stands for supersonic flow. The coefficients of the polynomials are constant parameters. The total angle of attack and angle-of-attack plane are defined in Eqs. (36) and (37), and α and β are angle of attack and sideslip angle, respectively.

References

[1] Korte, U., "Tasks and Needs of the Industrial Clearance Process," *Advanced Techniques for Clearance of Flight Control Laws*, Springer–Verlag, Berlin, 2002, pp. 13–33.

[2] Desai, P. N., Mitcheltree, R. A., and Cheatwood, F. M., "Entry Dispersion Analysis for the Stardust Comet Sample Return Capsule," AIAA Paper 1997-3182, 1997.

[3] Desai, P. N., and Cheatwood, F. M., "Entry Dispersion Analysis for the GENESIS Sample Return Capsule," *Journal of Spacecraft and Rockets*, Vol. 38, No. 3, 2001, pp. 345–350.

[4] Desai, P. N., and Knocke, P. C., "Mars Exploration Rovers Entry, Descent, and Landing Trajectory Analysis," AIAA Paper 2004-5092, 2004.

[5] Desai, P. N., Braun, R. D., Powell, R. W., Engelund, W. C., and Tartabin, P. V., "Six-Degree-of-Freedom Entry Dispersion Analysis for the METEOR Recovery Module," *Journal of Spacecraft and Rockets*, Vol. 34, No. 3, 1997, pp. 334–340.

[6] Fujita, K., Inatani, Y., and Hiraki, K., "Attitude Stability of Blunt-Body Capsules in Hypersonic Rarefied Regime," *Journal of Spacecraft and Rockets*, Vol. 41, No. 6, 2004, pp. 925–931. doi:10.2514/1.3588

[7] Winchenbach, G. L., Chapman, G. T., Hathaway, W. H., Ramsey, A., and Berner, C., "Dynamic Stability of Blunt Atmospheric Entry Configurations," *Journal of Spacecraft and Rockets*, Vol. 39, No. 1, 2002, pp. 49–55.

[8] Fielding, C., Varga, A., Bennani, S., and Selier, M., *Advanced Techniques for Clearance of Flight Control Laws*, Springer–Verlag, Berlin, 2002, pp. 4–33.

[9] Karlsson, F., and Fielding, C., "Industrial Evaluation," *Advanced Techniques for Clearance of Flight Control Laws*, Springer–Verlag, Berlin, 2002, pp. 433–445.

[10] Bates, D. G., and Postlethwaite, I., "The Structured Singular Value and μ Analysis," *Advanced Techniques for Clearance of Flight Control Laws*, Springer–Verlag, Berlin, 2002, pp. 37–55.

[11] Lowenberg, M., "Bifurcation and Continuation Method," *Advanced Techniques for Clearance of Flight Control Laws*, Springer–Verlag, Berlin, 2002, pp. 89–106.

[12] Verde, L., and Corraro, F., "Polynomial-Based Clearance of Eigenvalue Criteria," *Advanced Techniques for Clearance of Flight Control Laws*, Springer–Verlag, Berlin, 2002, pp. 333–353.

[13] Steele, J., and Vinnicombe, G., "ν-Gap Analysis of Stability Margin Criteria," *Advanced Techniques for Clearance of Flight Control Laws*, Springer–Verlag, Berlin, 2002, pp. 313–332.

[14] Varga, A., "Optimisation-Based Clearance," *Advanced Techniques for Clearance of Flight Control Laws*, Springer–Verlag, Berlin, 2002, pp. 107–117.

[15] Hansen, E., and Walster, G. W., *Global Optimization Using Interval Analysis*, Marcel Dekker, New York, 1992, pp. 1–13.

[16] Moore, R. E., *Interval Analysis*, Prentice–Hall, Upper Saddle River, NJ, 1966, pp. 1–14.

[17] Jaulin, L., Kieffer, M., Didrit, O., and Walter, E., *Applied Interval Analysis*, Springer–Verlag, London, 2001, pp. 54–63.

[18] Ratschek, H., and Rokne, J., *Computer Methods for the Range of Functions*, Horwood, Chichester, 1984, pp. 7–11.

[19] Kearfott, R. B., "Interval Arithmetic Methods for Nonlinear Systems and Nonlinear Optimization: an Outline and Status," *Impact of Recent Computer Advances on Operations Research*, Elsevier, Amsterdam, 1989, pp. 533–542.

[20] Neumaier, A., "Interval Iterations for Zeros of Systems of Equations," *BIT Numerical Mathematics*, Vol. 25, No. 1, March 1985, pp. 256–273. doi:10.1007/BF01935003.

[21] Jaulin, L., Kieffer, M., Didrit, O., and Walter, E., *Applied Interval Analysis*, Springer–Verlag, London, 2001, pp. 27–38.

[22] Jaulin, L., Kieffer, M., Didrit, O., and Walter, E., *Applied Interval Analysis*, Springer–Verlag, London, 2001, pp. 45–54.

[23] Doyle, J., "Analysis of Feedback Systems with Structured Uncertainties," *IEE Proceedings on Control Theory and Applications, Part D*, Vol. 129, No. 6, Nov. 1982, pp. 242–250.

[24] Safonov, M. G., "Stability Margins of Diagonally Perturbed Multivariable Feedback Systems," *IEE Proceedings on Control Theory and Applications, Part D*, Vol. 129, No. 6, Nov. 1982, pp. 251–256.

[25] Chang, B. C., Ekdal, O., Yeh, H. H., and Banda, S. S., "Computation of the Real Structured Singular Value via Polytopic Polynomial," *AIAA Journal of Guidance, Control, and Dynamics*, Vol. 14, No. 1, Jan.–Feb. 1991, pp. 140–147.

[26] Dailey, R., "A New Algorithm for the Real Structured Singular Value," *Proceedings of the American Control Conference*, International Federation of Automatic Control, Laxenburg, Austria, May 1990, pp. 3036–3040.

[27] Fu, M., and Dasgupta, S., "Computational Complexity of Real Structured Singular Value in ℓ_p Setting," *Transactions on Automatic Control*, Vol. 45, No. 11, Nov. 2000, pp. 2173–2176.

[28] Haddad, W. M., Chellaboina, V.-S., and Bernstein, D., "An Implicit Small Gain Condition and an Upper Bound for the Real Structured Singular Value," *Proceedings of the American Control Conference*,

International Federation of Automatic Control, Laxenburg, Austria, June 1997, pp. 2594–2598.

[29] Hayes, M. J., Bates, D. G., and Postlethwaite, I., "New Tools for Computing Tight Bounds on the Real Structured Singular Value," *AIAA Journal of Guidance, Control, and Dynamics*, Vol. 24, No. 6, Nov.–Dec. 2001, pp. 1204–1213.

[30] Sparks, A. G., and Bernstein, D. S., "Real Structured Singular Value Bounds using Rational Multipliers and Scaling," *Proceedings of the 34th Conference on Decision and Control*, Institute of Electrical and Electronics Engineers, New York, Dec. 1995, pp. 4343–4348.

[31] Juliana, S., Chu, Q. P., Mulder, J. A., and van Baten, T. J., "Flight Envelope Clearance of Atmospheric Re-entry Module with Flight Control," AIAA Paper 2004-5170, Aug. 2004.

[32] Juliana, S., Chu, Q. P., Mulder, J. A., and van Baten, T. J., "Systematic Approach of Worst Case Analysis on DART Re-entry Flight Envelope," *Proceedings of 4th International Symposium Atmospheric Re-entry Vehicles and Systems*, Session 13, Association Aeronautique and Astronautique of France, Paper 1, March 2005, pp. 1–7.

[33] Juliana, S., Chu, Q. P., Mulder, J. A., and van Baten, T. J., "Flight Control of Atmospheric Re-Entry Vehicle with Non-Linear Dynamic Inversion," AIAA Paper 2004-5330, Aug. 2004.

[34] Slotine, J.-J. E., and Li, W. P., "Feedback Linearization," *Applied Non-Linear Control*, Prentice–Hall, Upper Saddle River, NJ, 1991, pp. 207–271.

[35] La Salle, J., and Lefschetz, S., *Stability by Liapunov's Direct Method*, Academic Press, New York, 1961, pp. 37–40.